iScience

CellPress
OPEN ACCESS

Article

IFI-16 inhibition attenuates myocardial remodeling following myocardial infarction

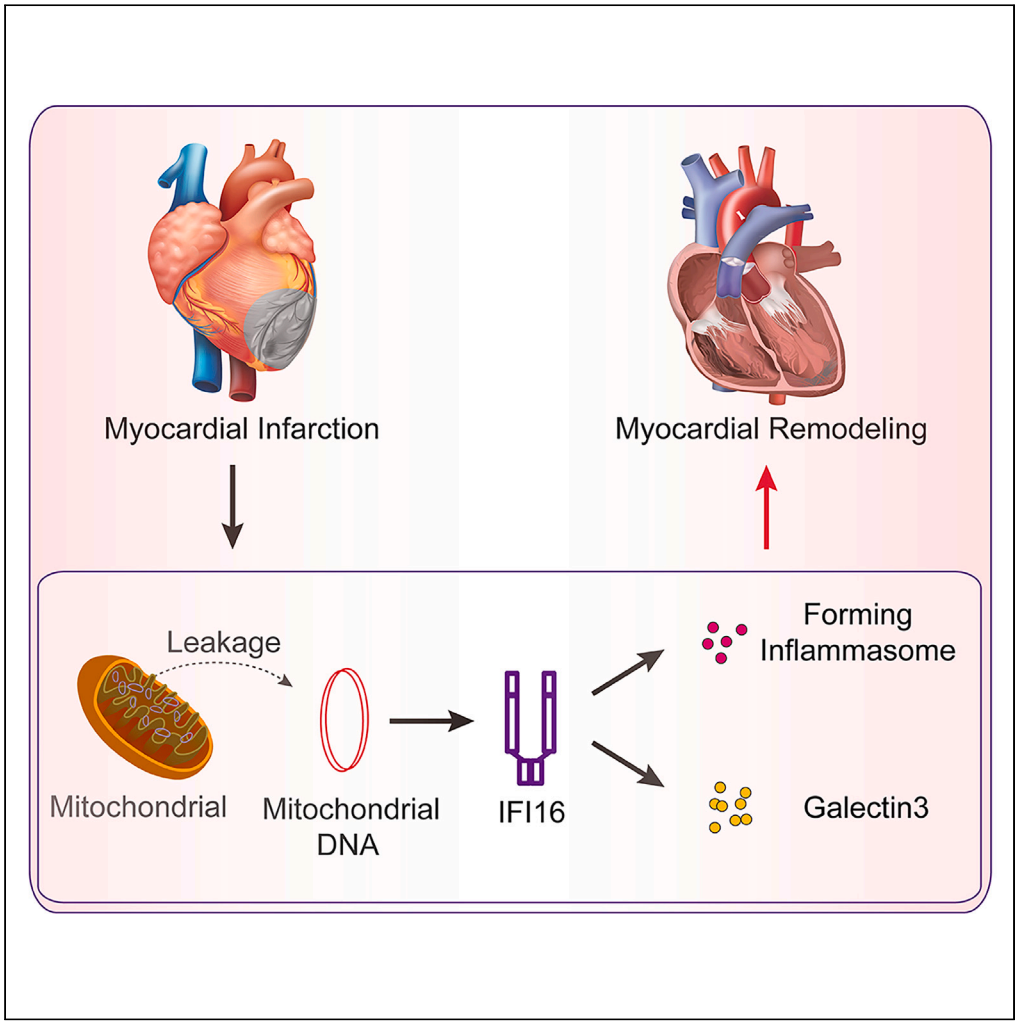

Yi Deng, Xiuqing Pang, Li Chen, ..., Jing Zeng, Yuchao Feng, Bojun Chen

speeters@126.com (Y.F.)
gzcbj@gzucm.edu.cn (B.C.)

Highlights

IFI-16 mediates inflammation in myocardial remodeling post-heart attack

IFI-16 interacts directly with galectin-3, crucial for inflammation regulation

Inhibiting IFI-16 is a promising therapy for managing myocardial remodeling

Deng et al., iScience 27, 110568
August 16, 2024
https://doi.org/10.1016/j.isci.2024.110568

iScience

CellPress
OPEN ACCESS

Article

IFI-16 inhibition attenuates myocardial remodeling following myocardial infarction

Yi Deng,[1,2,4,6] Xiuqing Pang,[5,6] Li Chen,[1,3,4,6] Weihang Peng,[1,3] Xiaoyan Huang,[1,3,4] Peiying Huang,[1,3,4] Shuai Zhao,[1,4] Zhishang Li,[1,4] Xingui Cai,[1,4] Qiuping Huang,[1,4] Jing Zeng,[1,4] Yuchao Feng,[1,3,4,*] and Bojun Chen[1,3,4,7,*]

SUMMARY

Myocardial remodeling (MR) following myocardial infarction (MI) contributes to heart failure. Inflammation is a key determinant in cardiac remodeling, with potential prognostic improvements by inhibiting inflammatory factors. Pattern recognition receptors, including interferon gamma-inducible protein-16 (IFI-16), play significant roles in this process, yet its specific involvement remains underexplored. This study investigates IFI-16's role in initiating inflammation via the inflammasome and its direct interaction with galectin-3 protein post-MI. Elevated IFI-16 levels were observed in human and rat myocytes and a mouse MI model under hypoxic, nutrient-deprived conditions, correlating with increased inflammation-associated proteins. Suppression of IFI-16/IFI-204 using short hairpin RNA (shRNA) lentivirus or adeno-associated virus decreased inflammatory factor activation, thereby mitigating remodeling and enhancing cardiac function post-MI. Co-immunoprecipitation (coIP) and double-fluorescence staining confirmed IFI-16's ability to interact directly with galectin-3. These findings underscore IFI-16's critical role as a pro-inflammatory factor in post-MI MR, suggesting its inhibition as a potential therapeutic strategy.

INTRODUCTION

Myocardial infarction (MI) is one of the most severe manifestations of coronary heart disease, posing a significant threat to human health. Following MI, the left ventricle (LV) undergoes a series of repair and wound healing responses, including inflammation and scar formation, collectively termed as LV remodeling. Prolonged and excessive LV remodeling can lead to HF post-MI, with a 5-year mortality rate of 50%.[1,2] Consequently, it is essential to improve our understanding of the cellular and molecular mechanisms that regulate post-MI LV remodeling.

Post-MI cardiac inflammation is initiated in response to ischemic stress and is triggered by the release of alarmins or damage-associated molecular patterns (DAMPs) from dying cardiomyocytes. DAMPs bind to specific pattern recognition receptors (PRRs) of the innate immune system found on parenchymal cells and infiltrating leukocytes. This activates the complement pathway and initiates an inflammatory cascade.[3–5] Substantial evidence highlights the crucial role of inflammation in cardiac remodeling post-MI.[6–8] In clinical practice, studies on canakinumab[9] and colchicine[10] have highlighted the feasibility and efficacy of anti-inflammatory therapies for the treatment of chronic coronary artery disease.

Interferon gamma inducible protein-16 (IFI-16) belongs to the PRR family and contains an N-terminal pyrin domain (PYD) and two C-terminal hematopoietic interferon-inducible nuclear domains.[11] IFI-16 has been implicated in inflammation, viral infections, innate immunity, and aging, suggesting its involvement in inflammation-associated human diseases.[12] Elevated IFI-16 levels have been observed in patients diagnosed with systemic lupus erythematosus and inflammatory bowel disease.[13,14] IFI-16 functions as a sensor of replicating DNA from herpes viruses in the nucleus. It forms an inflammasome complex consisting of IFI-16, apoptosis-associated speck-like protein containing a caspase recruitment domain, and caspase-1.[15] This assembly leads to the formation of the IFI-16-caspase-1 inflammasome complex. Furthermore, released mitochondrial DNA activates endothelial cells and promotes mitophagy through the IFI-16-NF-κB signaling pathway.[16] The murine ortholog of IFI-16, IFI-204, acts as a cytoplasmic DNA sensor, triggering stimulator of interferon genes (STING)-dependent type 1 interferon.[17,18] However, it's worth noting that there is a paucity of research concerning the function of IFI16 in cardiac physiology, and the specific

[1]The Second Clinical Medical School of Guangzhou University of Chinese Medicine, Guangzhou City, Guangdong Province 511400, China
[2]The Postdoctoral Research Station, Guangdong Provincial Hospital of Chinese Medicine, Guangzhou City, Guangdong Province 511400, China
[3]Guangdong Provincial Key Laboratory of Research on Emergency in Traditional Chinese Medicine, Clinical Research Team of Prevention and Treatment of Cardiac Emergencies with Traditional Chinese Medicine, Guangzhou City, Guangdong Province 511400, China
[4]Emergency Department of Guangdong Provincial Hospital of Traditional Chinese Medicine, Guangzhou City, Guangdong Province 511400, China
[5]Department of Infectious Diseases, the Third Affiliated Hospital of Sun Yat-sen University, 600 Tianhe Road, Guangzhou 510630, China
[6]These authors contributed equally
[7]Lead contact
*Correspondence: speeters@126.com (Y.F.), gzcbj@gzucm.edu.cn (B.C.)
https://doi.org/10.1016/j.isci.2024.110568

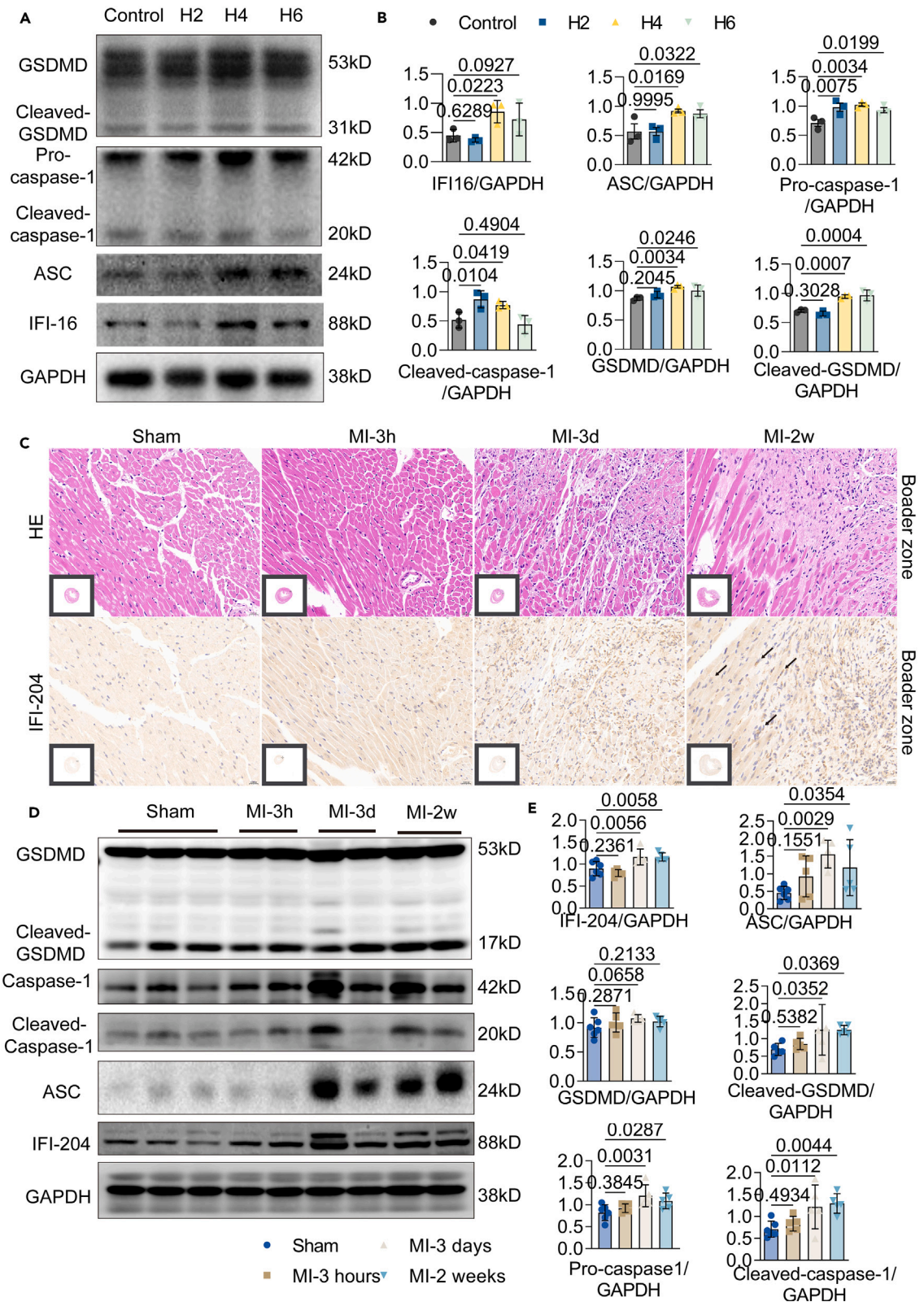
A
Control H2 H4 H6
GSDMD
Cleaved-GSDMD
Pro-caspase-1
Cleaved-caspase-1
ASC
IFI-16
GAPDH
53kD
31kD
42kD
20kD
24kD
88kD
38kD
B
Control H2 H4 H6
IFI16/GAPDH
ASC/GAPDH
Pro-caspase-1/GAPDH
Cleaved-caspase-1/GAPDH
GSDMD/GAPDH
Cleaved-GSDMD/GAPDH
C
Sham MI-3h MI-3d MI-2w
HE
IFI-204
Boader zone
Boader zone
D
Sham MI-3h MI-3d MI-2w
GSDMD
Cleaved-GSDMD
Caspase-1
Cleaved-Caspase-1
ASC
IFI-204
GAPDH
53kD
17kD
42kD
20kD
24kD
88kD
38kD
Sham
MI-3 hours
MI-3 days
MI-2 weeks
E
IFI-204/GAPDH
ASC/GAPDH
GSDMD/GAPDH
Cleaved-GSDMD/GAPDH
Pro-caspase1/GAPDH
Cleaved-caspase-1/GAPDH

Figure 1. Elevation of IFI-16/IFI-204 inflammasome following myocardial infarction

(A and B) Western blot analysis depicting the expression levels of IFI-16, ASC, pro-caspase-1, cleaved-caspase-1, GSDMD, and cleaved-GSDMD in AC16 myocytes exposed to hypoxia and nutrient deprivation for 0–6 h (control, H2, H4, and H6) with sample collection at the specified time points.

(C) Timeline outlining the collection of heart samples at 3 hours (3 h), 3 days (3 d), and 2 weeks (2 w) after ligation to establish a myocardial infarction (MI) mouse model. Sham heart samples were obtained at 2 weeks after surgery. Hematoxylin and eosin (H&E) staining, along with IFI204 immunostaining, was performed in a mouse MI model at different time points.

(D and E) Western blot analysis shows the expression of IFI-204, ASC, pro-caspase-1, cleaved-caspase-1, GSDMD, and cleaved-GSDMD in mouse heart tissue collected at different time points after coronary ligation and in sham-operated hearts. The western blot experiments were repeated three times, and the data are presented as mean ± SEM.

role of IFI-16 in post-MI cardiac remodeling remains elusive. This study investigated the role of IFI-16 in MR and explored the underlying mechanism of IFI-16 in post-MI procedures.

RESULTS

Elevation of IFI-16/IFI-204 inflammasome in cardiac remodeling post-MI

PRRs play a pivotal role in cardiac repair post-MI.[19] However, the role of IFI-16 in heart remodeling post-MI remains largely unknown. In our investigation, we systematically examined the expression levels of IFI-16, apoptosis-associated Speck-like protein (ASC), pro-caspase-1, cleaved-caspase-1, gasdermin-D (GSDMD), and cleaved-GSDMD over a time course under hypoxic and nutrient-deprived conditions in AC16 cells. The IFI-16 and tumor necrosis factor-α (TNF-α) levels exhibited a decline at 2 h (H2) of hypoxia and nutrient deprivation, followed by an elevation at 4 h (H4) and 6 h (H6) compared to the control group (Figures 1A and 1B). Notably, ASC, pro-caspase-1, GSDMD, and cleaved-GSDMD were activated between 2 and 6 h in the *in vitro* model, peaking at H4. While cleaved-caspase-1 levels increased at H4, they subsequently increased at H6 compared to the control group. Consequently, we focused our investigation on the 4-h hypoxia period. H9c2 cells in a hypoxic and nutrient deprivation model exhibited results consistent with those of AC16 cells (Figure S1). To verify the presence of IFI-16 and confirm the successful establishment of the MR mouse model, hearts were collected at predetermined time points. Subsequently, the samples were sectioned, and hematoxylin and eosin (H&E) staining and IFI-204 immunostaining were performed. The results revealed predominant IFI-204 expression in the infarcted area. Intriguingly, with the prolongation of MI duration, the expression of IFI-204 was found to progressively increase both in the infarcted area and in non-infarcted regions (Figures 1C, S2, and S3). Further assessment involved the examination of IFI-16, ASC, pro-caspase-1, cleaved-caspase-1, GSDMD, and cleaved-GSDMD in mouse models of MI (n = 5). IFI-204 and inflammasome-related proteins exhibited heightened expression three days post-infarction, with further increases observed at two weeks post-infarction (Figures 1D and 1E). Consequently, the two-week post-infarction heart remodeling model was selected for subsequent analysis.

IFI-16 recognition of mitochondrial released DNA

Our earlier findings demonstrated the upregulation of the IFI-16 inflammasome in MI models. Previous reports have established IFI-16 as a cytoplasmic DNA recognition receptor,[12] suggesting that impaired mitochondrial membrane integrity following MI results in leakage of mtDNA, which is subsequently recognized by IFI-16 in the cytoplasm, thereby promoting *IFI-16* expression. To explore this hypothesis, we examined total mtDNA levels in both the control group and the 4-h hypoxia and nutrient deprivation (H4) group in AC16 cells and observed an increase in mtDNA release under hypoxic conditions, consistent with the expression pattern of IFI-16 (Figure 2A; Table S1). To further investigate the relationship between mtDNA leakage and IFI-16 expression, we used VBIT4,[20] a suppressor of mtDNA leakage. The addition of VBIT4 decreased IFI-16 expression under H4 condition (Figures 2B and 2C); Table S1). Subsequently, we performed immunofluorescence labeling of mitochondria using Mito-Tracker-Rhodamine, and IFI-16 was labeled using fluorescein isothiocyanate (FITC). Our observations revealed a significant overlap between mitochondria and IFI-16, implying a close association between IFI-16 and mitochondrial activation (Figure 2D). These findings provide compelling evidence suggesting that the activation of IFI-16 is intricately linked to mitochondrial processes, specifically the recognition of leaked mtDNA.

IFI-16/Ifi-*204* knockdown suppresses inflammasome-associated protein activation post-MI

Building on our previous observations of elevated IFI-16 inflammasomes in MR post-MI, we hypothesized that the downregulation of *IFI-16* could diminish inflammasome-associated proteins and alleviate MR progression. We achieved *IFI-16* downregulation *in vitro* by lentivirus-mediated transfection of AC16 myocytes with the IFI16-shRNA-pLVX-PURO plasmid. Our results revealed a reduction in the levels of IFI-16, ASC, pro-caspase-1, cleaved-caspase-1, and cleaved-GSDMD during the 4-h period of hypoxia and nutrient deprivation (H4, see Figures 3A and 3B). To further investigate the role of IFI-16 *in vivo*, we employed adeno-associated viruses (AAVs) to knockdown *ifi-204*. As anticipated, the levels of ASC, cleaved-caspase-1, GSDMD, and cleaved-GSDMD were reduced in the AAV-IFI204 (pAAV-U6-shRNA (*ifi204*)-CMV-EGFP-WPRE) group compared to the AAV-Ctrl (pAAV-U6-shRNA (NC2)-CMV-EGFP-WPRE) group (Figures 3C and 3D; Figure S7). These results are consistent with those observed in the *in vitro* study. Subsequent investigations using wheat germ agglutinin (WGA) fluorescence staining and tissue-specific immunofluorescence staining revealed significant disparities. Specifically, the average fluorescence intensity of Cy3-labeled IFI-204 was significantly lower in the AAV-IFI204 group compared to the AAV-Ctrl group (Figures 3E and 3F; Figure S4). Overall, these findings suggest that the downregulation of *IFI-16* leads to decreased expression of various inflammasome-associated proteins, thereby indicating the potential role of IFI-16 in modulating the inflammatory response and attenuating MR post MI.

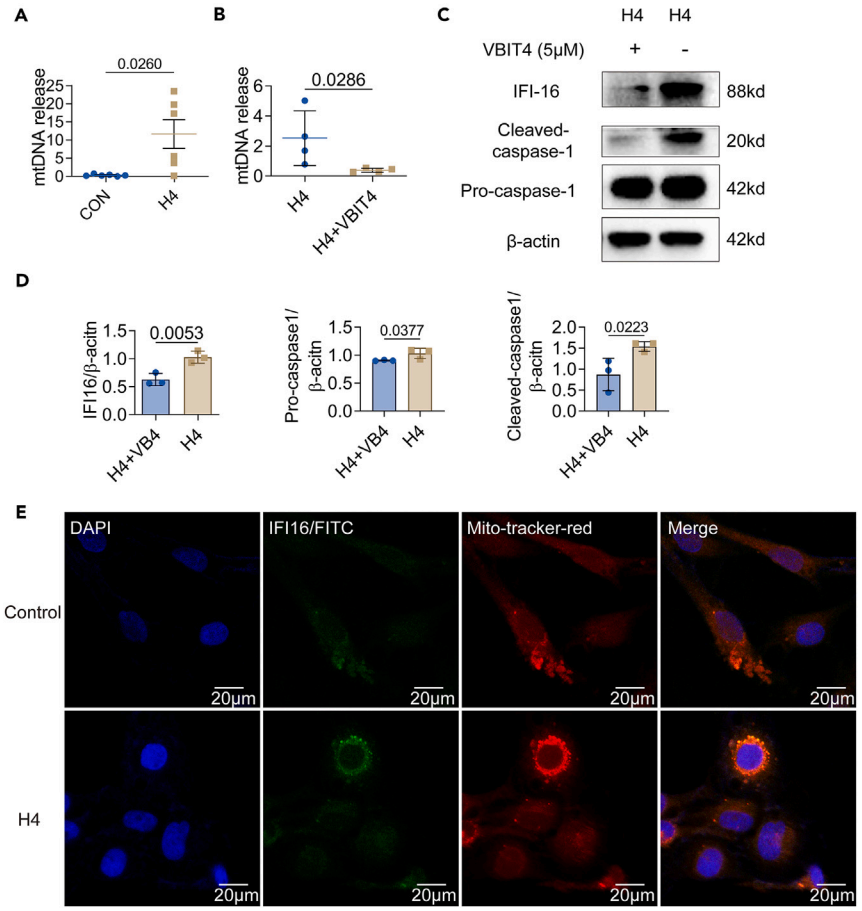

Figure 2. IFI-16 recognition of mitochondrial released DNA

(A) Quantification of released mitochondrial DNA copy number in AC16 myocytes exposed to hypoxia and nutrient deprivation for 4 h (H4) compared to the normal control (Con) using qPCR with D loop1, a mitochondrial DNA-specific primer.

(B) Measurement of mitochondrial DNA leakage in hypoxia and nutrient deprivation for 4 h (H4) with or without VBIT4 treatment (5 μM).

(C and D) Western blot analysis illustrating the expression levels of IFI-16, cleaved-caspase-1, and pro-caspase-1 in AC16 myocytes in hypoxia and nutrient deprivation for 4 h (H4) with or without VBIT4 treatment.

(E) Immunofluorescence staining displaying the localization of IFI-16 (labeled with FITC-tagged secondary antibody) and mitochondria (labeled with mito-tracker-red) in hypoxia and nutrient deprivation for 4 h and normal control in AC16 cells. Western blot experiments were repeated three times, and data are presented as mean ± SEM.

Knockdown of *IFI-16/Ifi-204* reduces apoptosis in tissues and cells post-MI

Studies have shown that IFI-16 can activate apoptosis through p53.[21] Apoptosis is recognized as a prominent mechanism of cell death in MI. Consequently, we hypothesized that the knockdown of *IFI-16* and *Ifi-204* would lead to a reduction in apoptosis in both cells and myocardial tissues. To investigate this, we assessed the expression of p53 and cleaved-caspase-9 in *IFI-16* knockdown cardiomyocytes by western blotting. The results revealed a significant decrease in p53 and cleaved-caspase-9 expression in the short hairpin RNA (shRNA) group compared to the scrambled group (Figure 4B). Subsequently, TUNEL staining was performed on the cells, demonstrating a lower proportion of red-positive cells in the shRNA group compared to the scramble group (Figure 4A). These findings were consistent with the TUNEL assay and p53 and cleaved-caspase-9 expressions examined *in vivo*. Following the knockdown of *Ifi-204*, the expression of p53 and cleaved-caspase-9 and the positive ratio of TUNEL decreased (Figures 4C and 4D). Collectively, these results suggested that *IFI-16* knockdown led to reduced myocardial apoptosis during the remodeling procedure post-MI.

Ifi-204 knockdown improves heart function and attenuates remodeling post myocardial infarction

To further elucidate the role of IFI-16 (mouse IFI-204) in cardiac function, cardiac ultrasound examinations were conducted two weeks post-surgery. The results demonstrated a significant enhancement in the ejection fraction (EF) and fractional shortening (FS) in the AAV-IFI204 group compared to those in the AAV-Ctrl group (Figure 5A; Figures S5 andS10). Subsequently, mouse hearts were harvested, and Masson's trichrome and H&E staining were performed on cardiac tissue sections (Figures 5B and 5C). The findings revealed a substantial

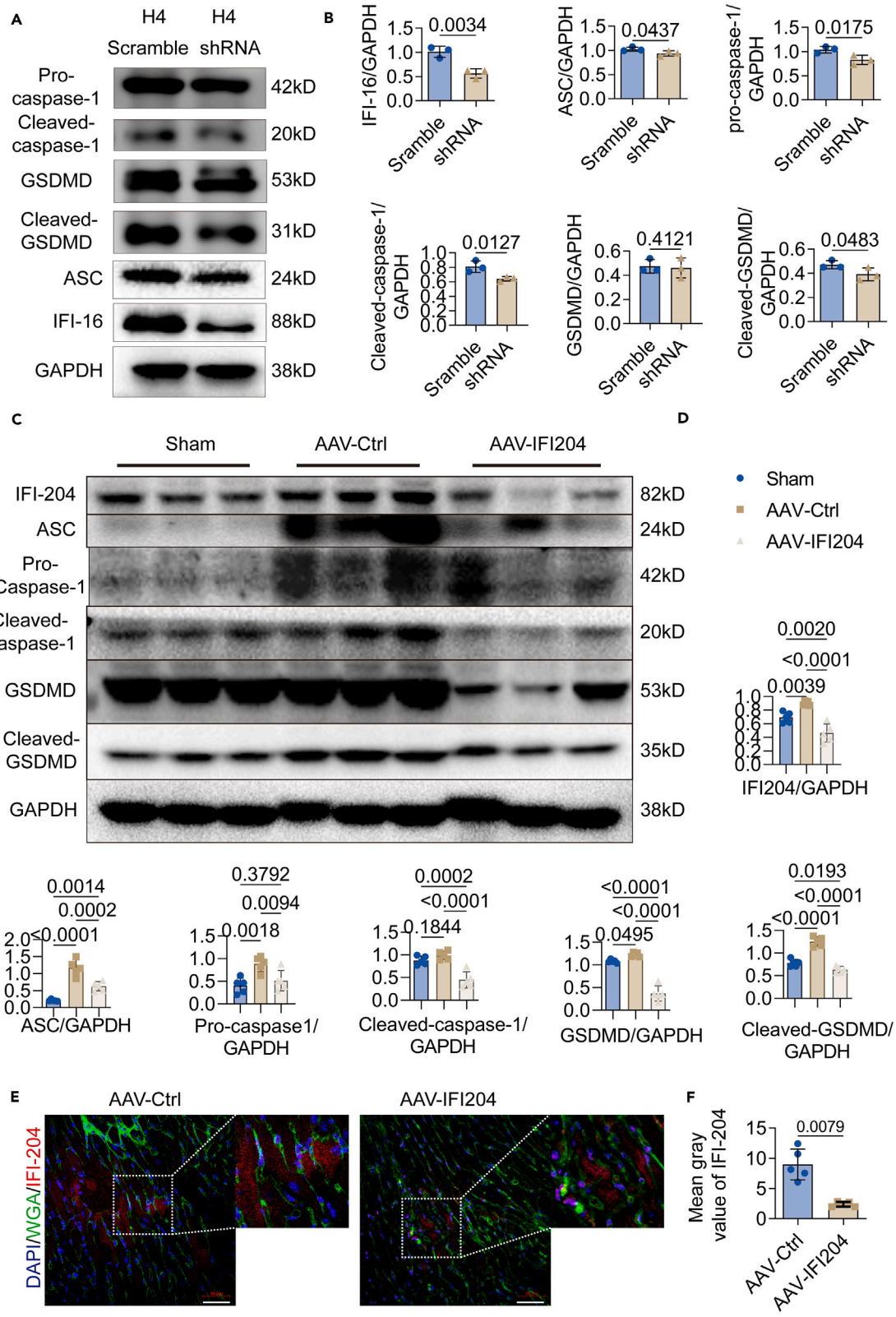
A
H4
Scramble
H4
shRNA
Pro-caspase-1
42kD
Cleaved-caspase-1
20kD
GSDMD
53kD
Cleaved-GSDMD
31kD
ASC
24kD
IFI-16
88kD
GAPDH
38kD
B
IFI-16/GAPDH
0.0034
ASC/GAPDH
0.0437
pro-caspase-1/GAPDH
0.0175
Cleaved-caspase-1/GAPDH
0.0127
GSDMD/GAPDH
0.4121
Cleaved-GSDMD/GAPDH
0.0483
Sramble
shRNA
C
Sham
AAV-Ctrl
AAV-IFI204
IFI-204
82kD
ASC
24kD
Pro-Caspase-1
42kD
Cleaved-Caspase-1
20kD
GSDMD
53kD
Cleaved-GSDMD
35kD
GAPDH
38kD
D
Sham
AAV-Ctrl
AAV-IFI204
IFI204/GAPDH
0.0020
<0.0001
0.0039
ASC/GAPDH
0.0014
0.0002
<0.0001
Pro-caspase1/GAPDH
0.3792
0.0094
0.0018
Cleaved-caspase-1/GAPDH
0.0002
<0.0001
0.1844
GSDMD/GAPDH
<0.0001
<0.0001
0.0495
Cleaved-GSDMD/GAPDH
0.0193
<0.0001
<0.0001
E
AAV-Ctrl
AAV-IFI204
DAPI/WGA/IFI-204
F
Mean gray value of IFI-204
0.0079
AAV-Ctrl
AAV-IFI204

Figure 3. IFI-16/IFI-204 knockdown suppress inflammasome-associated proteins activation following myocardial infarction

(A and B) Myocytes were transfected with the lentivirus, ifi16-shRNA, to knock down IFI-16 expression, followed by exposure to hypoxia and nutrient deprivation for 4 h (H4). Scramble-shRNA was used as control. Western blot analysis was performed to assess the levels of IFI-16, ASC, pro-caspase-1, cleaved-caspase-1, GSDMD, and cleaved-GSDMD.

(C and D) Injection of adeno-associated virus (AAVs) to knock down ifi204 expression in mice was used, with AAV-Ctrl injection serving as the normal control. Two weeks after surgery, hearts were harvested for further examination after ultrasound echocardiography. Western blot analysis of IFI-16, ASC, pro-caspase-1, cleaved-caspase-1, GSDMD, and cleaved-GSDMD expression in heart tissue obtained from mice in the different treatment groups.

(E) The assessment of IFI-204 expression within tissues was conducted through immunofluorescence analysis. In this analysis, green fluorescence signified wheat germ agglutinin (WGA), blue fluorescence represented DAPI staining, and red fluorescence indicated the presence of Cy3-labeled IFI-204. Scale bar: 50 μm.

(F) Quantitative assessment of the mean fluorescence intensity for each respective group in (E) was conducted. Western blot experiments were repeated three times, and data are presented as mean ± SEM.

decrease in the fibrotic area in the AAV-IFI204 group compared to the AAV-Ctrl group (n = 5). Furthermore, H&E staining demonstrated a significant improvement in the distribution of myocardial inflammatory cells in the AAV-IFI204 group compared to that in the AAV-Ctrl group (Figures 5D and 5E). The expression levels of TNF-α and α-SMA in the AAV-Ctrl and AAV-IFI204 groups were assessed through

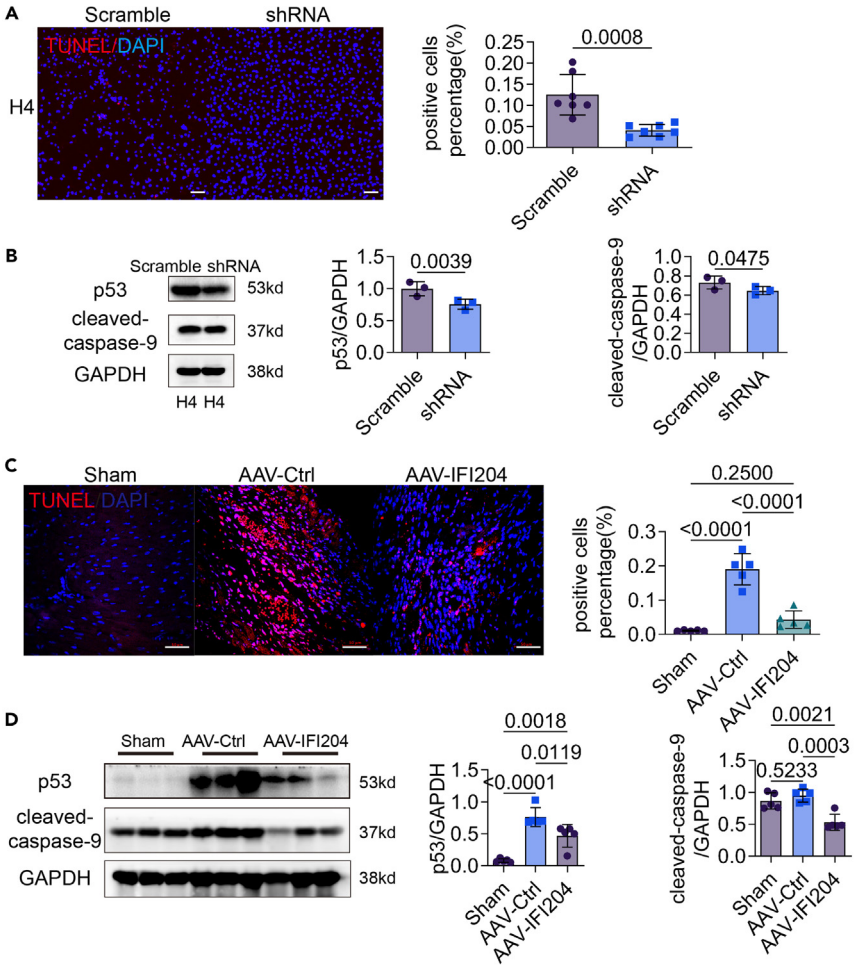

Figure 4. Knockdown of IFI-16/IFI-204 reduces apoptosis in tissues and cells after myocardial infarction

(A) TUNEL detection in myocytes. Lentiviral transfection was utilized to knock down IFI-16 in AC16 cells. Subsequently, TUNEL detection was performed after 4 h of hypoxia and nutrient deprivation (H4). Images captured via laser confocal microscopy depict blue fluorescence for DAPI and red fluorescence for TUNEL-positive cells. Scale bar: 100 μm. Statistical analysis was conducted using ImageJ.

(B) Western blot analysis was performed to evaluate the expression of p53 and cleaved caspase-9 in myocytes in both the scramble and shRNA groups.

(C) TUNEL staining was conducted on cardiac slices from the sham group, AAV-Ctrl group, and AAV-IFI204 group. Laser confocal microscopy captured images, and statistical analysis was performed using ImageJ. Scale bar: 50 μm.

(D) Western blot detection and statistical analysis were employed to assess the expression of p53 and cleaved-caspase-9 in the sham group, AAV-Ctrl group, and AAV-IFI204 group. The western blot experiments were replicated three times, and data are presented as mean ± SEM.

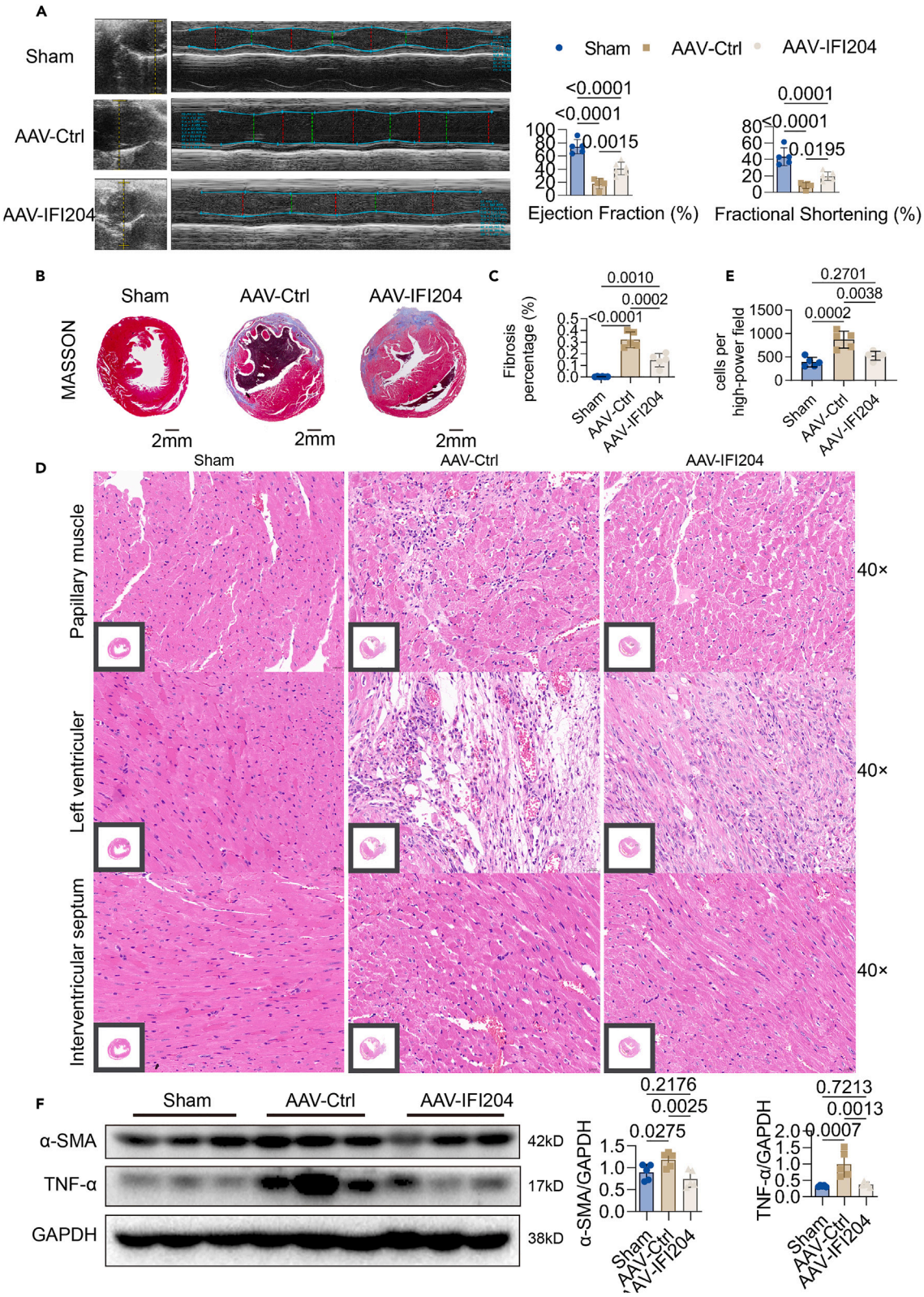
A
Sham
AAV-Ctrl
AAV-IFI204
Sham
AAV-Ctrl
AAV-IFI204
<0.0001
<0.0001
0.0015
Ejection Fraction (%)
0.0001
<0.0001
0.0195
Fractional Shortening (%)
B
MASSON
Sham
AAV-Ctrl
AAV-IFI204
2mm
2mm
2mm
C
Fibrosis percentage (%)
0.0010
0.0002
<0.0001
Sham
AAV-Ctrl
AAV-IFI204
E
cells per high-power field
0.2701
0.0038
0.0002
Sham
AAV-Ctrl
AAV-IFI204
D
Sham
AAV-Ctrl
AAV-IFI204
Papillary muscle
Left ventricular
Interventricular septum
40×
40×
40×
F
Sham
AAV-Ctrl
AAV-IFI204
α-SMA
TNF-α
GAPDH
42kD
17kD
38kD
0.2176
0.0025
0.0275
α-SMA/GAPDH
Sham
AAV-Ctrl
AAV-IFI204
0.7213
0.0013
0.0007
TNF-α/GAPDH
Sham
AAV-Ctrl
AAV-IFI204

Figure 5. IFI-204 knockdown improves heart function and attenuates remodeling post myocardial infarction

(A) Two weeks post-surgery, mice were anesthetized with pentobarbital (50 mg/kg) for echocardiography. Parasternal short axis view and parasternal long axis view images were obtained. Statistical analysis of echocardiography data was performed in the sham, AAV-Ctrl, and AAV-IFI204 groups (n = 5 in each group).

(B and C) Images of Masson staining in the sham, AAV-Ctrl, and AAV-IFI204 groups (n = 5) were captured. Statistical analysis of fibrosis proportion in Masson-stained samples was conducted.

(D and E) Images of H&E staining in the sham, AAV-Ctrl, and AAV-IFI204 groups (n = 5) were obtained, and statistical analysis of the number of cells within the field of view was conducted.

(F) Western blot analysis was performed to assess TNF-α and α-SMA expression in heart tissue obtained from mice in the Sham, AAV-Ctrl, and AAV-IFI204 groups. Data are presented as mean ± SEM.

western blot analysis (Figure 5F), indicating a reduction in TNF-α and α-SMA levels in the AAV-IFI204 group compared to the AAV-Ctrl group.

In conclusion, the downregulation of *Ifi-204* not only improved cardiac function and reduced fibrosis but also attenuated the expression of inflammatory markers, suggesting a potential therapeutic strategy to mitigating remodeling post-MI.

Galectin-3 and IFI-16 expression is correlated

To further investigate the mechanistic role of IFI-16, we performed RNA sequencing after overexpressing *IFI-16*. Pearson's correlation analysis confirmed a robust correlation between the samples (Figure 6A). The results revealed 189 upregulated and 21 downregulated genes in the *IFI-16* overexpression group (Figure 6B; Table S2). To understand the functional implications of these differentially expressed genes, we performed Gene Ontology (GO) enrichment analysis, which revealed a significant association with myocardial ischemia for most genes (Figures 6C; Table S3). Notably, *LGALS3* (galectin-3) emerged as a significantly upregulated gene in this context (Figure 6D).

Previous research indicates that galectin-3 promotes inflammation and fibrosis and can serve as an indicator of the severity of HF. Evaluating the expression of galectin-3 in a post-MI MR model, revealed a pattern consistent with *IFI-16* expression. Furthermore, we examined the expression of galectin-3 in an MR mouse model with downregulated *IFI-16* and found a high degree of consistency with *IFI-16* expression (Figures 6E and 6L). Using western blotting, we conducted a correlation analysis between the expression of IFI-16 and galectin-3, revealing a possible correlation between the two proteins, with an R square = 0.5228, $p < 0.0001$ (Figure 6M). This suggests a potential association between galectin-3 and *IFI-16* expression.

Direct combination of IFI-16 and galectin-3

To elucidate the potential interrelationship between IFI-16 and galectin-3, we conducted co-immunoprecipitation (coIP) experiments using AC16 cells, which demonstrated that IFI-16 can precipitate galectin-3, as illustrated in Figures 7A and S9. Subsequently, we investigated IFI-16's capacity to pull down galectin-3 under normal culture conditions (Con) and during hypoxia and nutrient deprivation for 4 h (H4). Interestingly, we observed that at H4, IFI-16's ability to pull down galectin-3 differs between the normal group and the H4 group (Figure 7B). Fluorescence labeling of IFI-16 and galectin-3 in AC16 cells and mouse heart slices revealed substantial co-localization of these two proteins (Figures 7C and 7D; Figure S6), providing compelling evidence of a direct interaction between them. To further elucidate the relationship between IFI-16 and galectin-3, we performed plasmid overexpression of IFI-16 (OV-IFI16) and small interfering RNA (siRNA) interference targeting galectin-3 (siRNA-Gal). Con-siRNA and Con-OV served as the negative control group. Results revealed that siRNA effectively downregulates galectin-3 expression in the H4 background, while overexpression (OV) enhances IFI-16 expression under H4 conditions. In the siRNA group, levels of caspase-1, cleaved-caspase-1, GSDMD, and cleaved-GSDMD were significantly lower compared to the con-siRNA group. Conversely, in the OV-IFI16 group, these proteins exhibited higher expression levels compared to the con-OV group. The OV-IFI16+siRNA-Gal group showed protein expression levels similar to the OV-IFI16 group, which were higher than those in the siRNA-Gal group. However, notable differences were observed in the protein expression levels of ASC, cleaved-caspase-1, GSDMD, and cleaved-GSDMD between the OV-IFI16 and OV-IFI16+siRNA-Gal groups.

Using molecular docking methods, we predicted the binding interaction between IFI-16 and galectin-3, revealing a calculated binding free energy of −22.8348 kcal/mol (Figure 7E; Figure S8). These findings suggest that galectin-3 interacts directly with IFI-16, potentially acting as a crucial mediator of IFI-16 and exerting pro-inflammatory and pro-fibrotic roles in the context of post-MI remodeling. In summary, the upregulation of *IFI-16* leads to altered gene expression, particularly of genes associated with inflammation, and the direct interaction between IFI-16 and galectin-3 contributes to the pro-inflammatory and pro-fibrotic processes observed during MR after infarction.

DISCUSSION

Recent research has provided compelling evidence implicating inflammation in cardiac remodeling following ischemic heart disease, particularly MI. Various PRRs, such as NOD-like receptor protein 3 (NLRP3),[22] absent in melanoma 2 (AIM2),[23] toll-like receptor 2 (TLR2),[24] toll-like receptor 9 (TLR9),[25,26] and cyclic guanosine monophosphate-adenosine monophosphate synthase (cGAS)[27] have been shown to play important roles in MR post-infarction. However, the role of IFI-16, a type of PRR,[16,28] in the heart, particularly in MR, has been poorly investigated. In this study, we demonstrate that IFI-16 is upregulated during MR post-infarction, and knocking down *IFI-16* results in a decrease in ASC-caspase-1 signaling and cleaved-GSDMD, TNF-α, and α-SMA levels during MR. These findings indicate a key role of IFI-16 in regulating inflammation during cardiac repair post-MI.

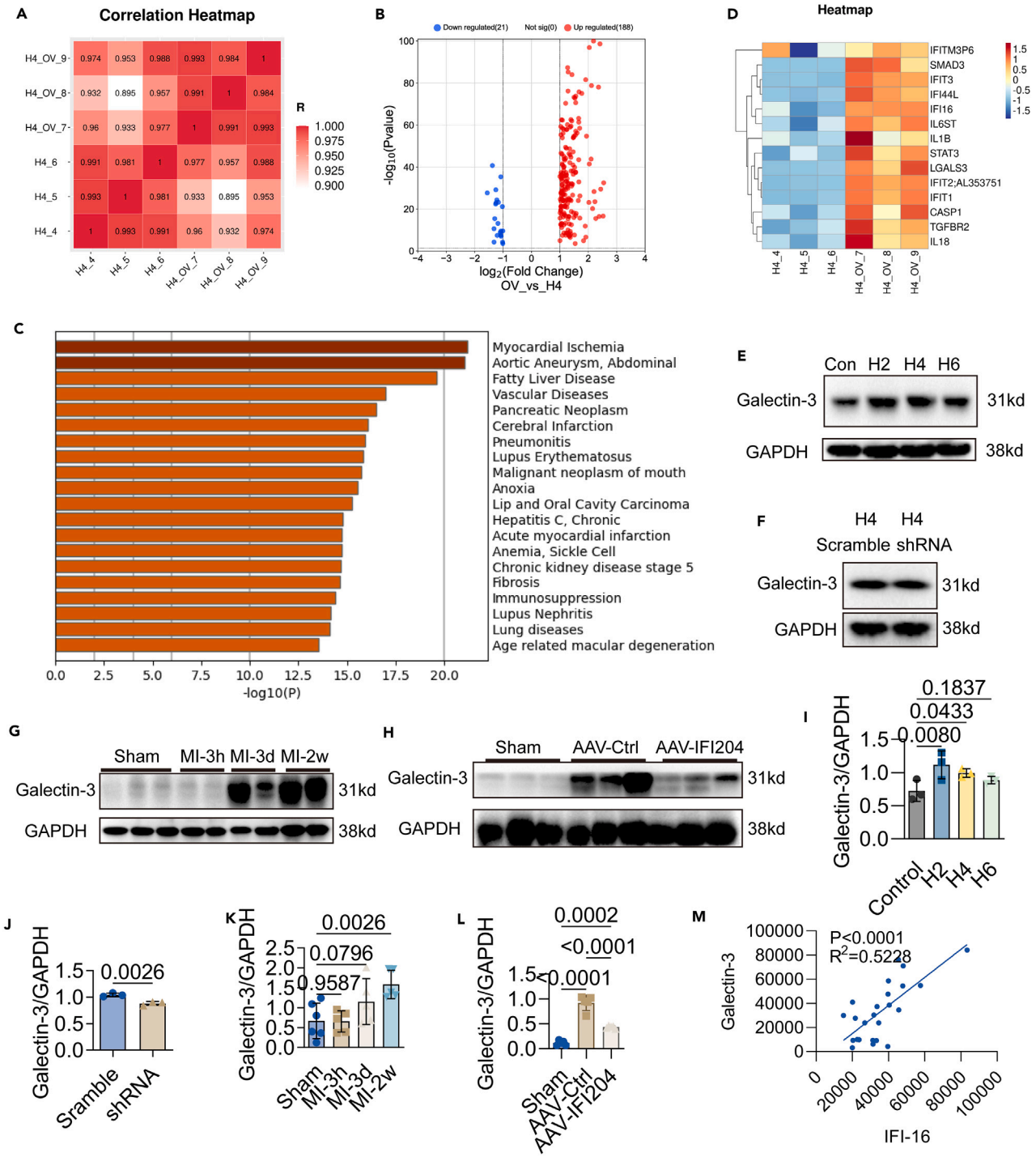

Figure 6. Consistent expression trends of IFI-16 and galectin-3

(A) Pearson correlation heatmap illustrates the repeatability of samples within and between groups in myocytes overexpressing (OV) IFI-16 with the IFI16-pcdh-GFP+PURO plasmid compared to the control group using the pcdh-GFP+PURO plasmid (n = 3), all samples were subjected to 4-h hypoxia and nutrient deprivation (H4).

(B) Volcano plots depict the differentially expressed genes between the OV-H4 and H4 groups. Red and green dots represent up-regulated (189 dots) and down-regulated (21 dots) transcripts, respectively ($p < 0.05$, [log2fc] > 1).

(C) An analysis of disease association was performed on the different genes using disgenet.

(D) Heatmap displays myocardial ischemia-related genes between the OV-H4 and Vector-H4 groups.

Figure 6. *Continued*

(E and I) Western blot analysis of galectin-3 expression in AC16 myocytes during the *in vitro* hypoxia and nutrient deprivation for 0–6 h.

(F and J) Western blot analysis of galectin-3 expression in IFI-16 knockdown AC16 cells in 4 h of hypoxia and nutrient deprivation *in vitro* model (H4).

(G and K) Western blot analysis of galectin-3 expression in the hearts of the post-infarction myocardial remodeling mouse model.

(H and L) Western blot analysis of galectin-3 expression in the hearts of IFI-16 knockdown mouse models.

(M) A correlation analysis was performed to assess the relationship between IFI-16 and galectin-3 expression. Data are presented as mean ± SEM.

Our findings reveal that IFI-16 predominantly localizes in the cytoplasm of AC16 myocytes, in contrast to its distribution in vascular smooth muscle cells.[29] This difference suggests that IFI-16 may assume different roles depending on the cell-type. In human macrophages, IFI-16 detects HIV proviral DNA and activates cGAS, a stimulator of interferon genes (STING), and type I interferon production.[30] Although IFI-16 increases cyclic guanosine monophosphate-adenosine monophosphate (cGAMP) production by cGAS in macrophages, it does not exhibit this activity in keratinocytes. This observation emphasizes the cell-specific roles of IFI-16 in its interaction with the cGAS pathway.[31] AIM2 and IFI-16 belong to the PYD 200 family, and AIM2 is mainly expressed in the cytoplasm of myocardial cells.[32] These were consistent with our results.

During conditions of hypoxia or ischemia, myocyte death leads to the release of DAMPs.[33] mtDNA has been described as a DAMP[34]; it is the primary source of DNA in the cytoplasm. In response to cellular injury, it leaks out through the mitochondrial permeability transition pore (mPTP)[35] or through mitochondrial outer membrane permeabilization (MOMP) mechanisms, such as BAX/BAK oligomers[36] and voltage-dependent anion-selective channels (VDACs).[20] IFI-16 is a viral DNA sensor involved in innate immune signaling. Our findings show that IFI-16 is located in the cytoplasm of myocytes, where mtDNA is primarily present. Hypoxia induces the release of mtDNA. Furthermore, we confirmed the co-localization of IFI-16 and mitochondria under hypoxic conditions. These results suggest that IFI-16 is activated by mtDNA leakage post-MI.

Previous studies have shown that NLRP3 induces inflammation in MR models activated by leaked mtDNA.[37] Another study demonstrated that damaged mtDNA released from pressure-overloaded cardiomyocytes activates TLR9 and induces sterile inflammation, leading to left ventricular failure.[25] Inflammasome activation, characterized by the activation of AIM2 and NLRC4 inflammasomes, has also been observed in chronic HF; AIM2 inhibition has been proposed as a therapeutic strategy for the treatment of chronic HF.[23] These findings are consistent with our results and support the notion that injured mitochondria release DAMPs, triggering inflammation during cardiac remodeling.

In $CD4^+$ T cells, IFI-16 forms an inflammasome complex with ASC, leading to the activation of caspase-1 and subsequent pyroptotic cell death, which effectively aborts the infection within these cells.[38] IFI-16 proteins are also involved in the activation of the cGAS/STING pathway, which induces the expression of type I interferon (IFN-β) in response to cytosolic DNA.[39] Previous investigations have demonstrated the activation of the cGAS/STING pathway during pressure overload, and inhibition of this pathway prevents pathological cardiac remodeling and left ventricular dysfunction under pressure overload conditions.[40] Our results indicate that *IFI-16* knockdown in mouse models of post-infarction MR improves heart function by reducing myocardial fibrosis and inflammation. Specifically, the downregulation of IFI-16 is associated with decreased levels of ASC, cleaved caspase-1, GSDMD-N, and IL-1β, which are components of the inflammasome, as well as downstream inflammatory factors. These findings are consistent with previous investigations involving the knockdown or knockout of NLRP3 and TLR9 in MR procedures.[25,37] IFI-16 has been reported to activate apoptosis through p53[21]; our results indicate that IFI-16 regulates apoptosis through the p53/cleaved caspase-9 pathway.

To gain further insights into the association between IFI-16 and MR, we performed mRNA sequencing using an *in vitro* MR model. Our data revealed that many differentially expressed genes are associated with inflammation. Notably, *LGALS3* (galectin-3) emerged as one of the 50 most significant genes between the overexpression and control groups. Galectin-3, a 35 kDa protein encoded by the *LGALS3* gene located on chromosome 14,[41] is a beta-galactoside-binding lectin that plays a pivotal role in fibrosis formation in multiple organs. It is involved in cardiac fibrosis in the context of pressure overload, hypertension, and post-MI remodeling.[42] Furthermore, it has emerged as a biomarker of fibrosis in heart diseases,[43] with elevated baseline levels in healthy individuals associated with increased mortality.[44,45] Mechanistically, *in vitro* studies have demonstrated that galectin-3 can induce the differentiation of quiescent fibroblasts into myofibroblasts, which produce and secrete matrix proteins, including collagens, fibronectin, and TGF-β.[46] Furthermore, *in vivo* studies have demonstrated the important role of galectin-3 in cardiac fibrosis and remodeling. Studies using hypertensive rats have revealed that galectin-3 co-localizes with macrophages and fibroblasts in fibrotic areas,[46] while experiments involving hypertensive rats and mice subjected to pressure overload have demonstrated that the absence of galectin-3 prevents cardiac fibrosis and is associated with reduced α-SMA staining (indicative of myofibroblast proliferation), decreased proliferating cells, and reduced fibrosis.[47] Moreover, IFI-16 contributes to the onset of cellular senescence, which is associated with beta-galactosidase.[48] Consistent with these findings, our results demonstrate elevated galectin-3 levels in the *in vitro* and *in vivo* MR models, which decreased upon *IFI-16* knockdown. In pursuit of a comprehensive understanding of the intricate interplay between IFI-16 and galectin-3, our coIP investigations provided compelling evidence of the intrinsic capability of IFI-16 to effectively co-precipitate galectin-3. Moreover, fluorescence labeling studies elucidated the distinct co-localization of these two proteins, substantiating their direct interaction. Nevertheless, further research is warranted to elucidate the specific mechanistic underpinnings and their impact on protein function. These findings propose that galectin-3 is a pivotal mediator of IFI-16, contributing to the observed pro-inflammatory and pro-fibrotic effects on MR following infarction.

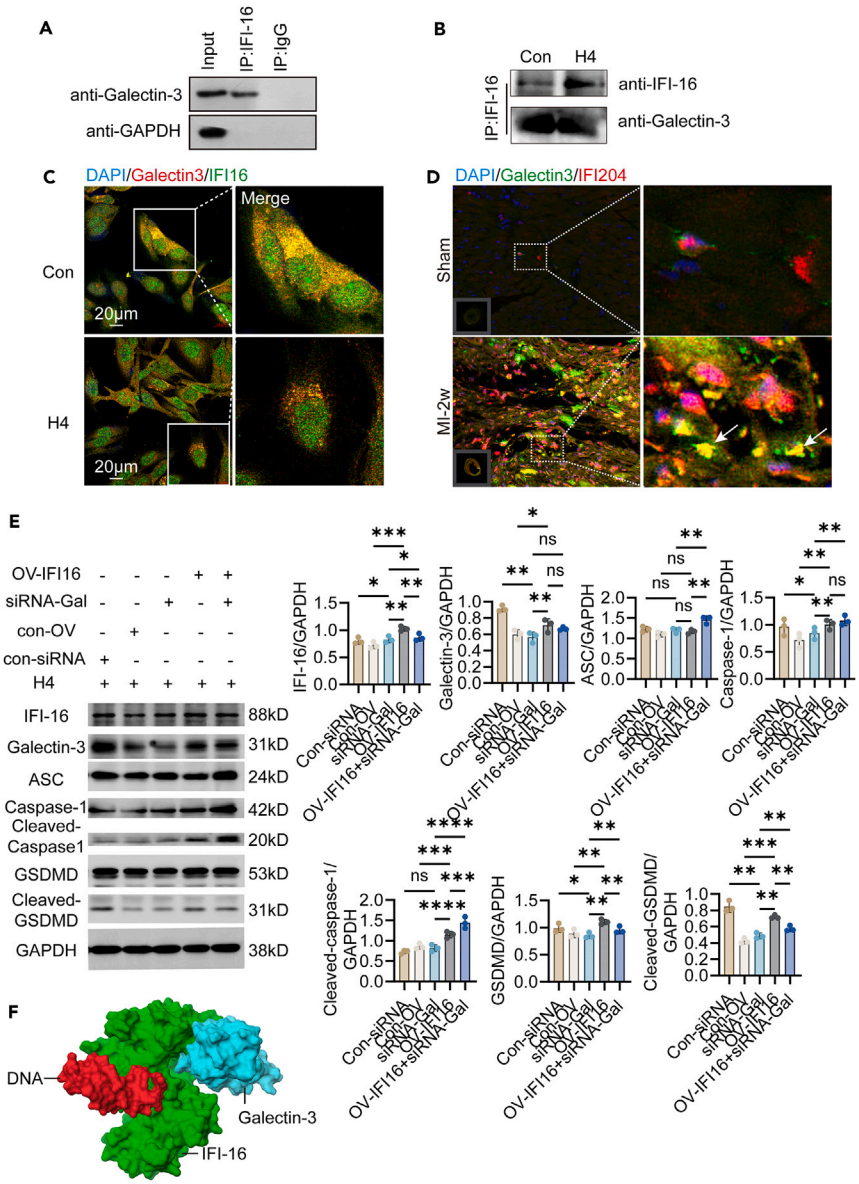

Figure 7. IFI-16 combines to galectin-3 directly

(A and B) Western blot analysis of co-immunoprecipitated products.

(A) The eluted products obtained from co-immunoprecipitation (coIP) were subjected to western blot detection for GAPDH and galectin-3.

(B) The eluted products were subjected to western blot detection for IFI-16 and galectin-3.

(C) Fluorescence double staining analysis in AC16 cells. Galectin-3 was labeled using a Cy3 secondary antibody, while IFI16 was labeled with an FITC secondary antibody. DAPI staining was additionally employed. The images were captured using laser confocal microscopy.

(D) Fluorescence double staining analysis in heart slices. Galectin-3 was labeled using an FITC secondary antibody, while IFI16 was labeled with a Cy3 secondary antibody. DAPI staining was additionally employed. The images were magnified by a factor of 63×.

(E) Overexpressing (OV) IFI-16 with the IFI16-pcdh-GFP+PURO plasmid and siRNA-mediated interference with galectin-3 expression. Con-siRNA and Con-OV served as the negative control group. Western blot analysis was performed to assess the levels of IFI-16, galectin3, ASC, pro-caspase-1, cleaved-caspase-1, GSDMD, and cleaved-GSDMD. * represents $p < 0.05$, ** represents $p < 0.01$, *** represents $p < 0.001$, **** represents $p < 0.0001$. Data are presented as mean ± SEM.

(F) Molecular docking pattern. A diagram illustrating the molecular docking pattern was created. Protein structures 2nmn (galectin-3) and 4qgu (IFI-16-DNA) were obtained from the Protein DataBank (PDB). Molecular docking experiments were conducted using Schrödinger's protein-protein docking module. In the visual representation, the 4qgu protein is depicted with green ribbons, the nucleic acid structure with red ribbons, and the 2nmn protein structure with blue ribbons.

In conclusion, our study highlights the role of IFI-16 in promoting inflammation during the cardiac remodeling post-MI. IFI-16 knockdown alleviates MR and improves heart function in a post-infarction setting by exerting anti-inflammatory effects. Galectin-3 has emerged as a direct signaling molecule of IFI-16 and may act as a key mediator of IFI-16-induced proinflammatory and profibrotic processes. However, the exact mechanism underlying the regulation of galectin-3 by IFI-16 requires further investigation.

Limitations of the study

In our study, we utilized adeno-associated virus to knock down IFI-204 *in vivo* and conducted subsequent experimental validations. Using transgenic mice with cardiac-specific IFI-204 knockout might provide a better understanding of the mechanistic role of IFI-204. Additionally, our research demonstrated an interaction between IFI16 and galectin-3 proteins. However, the detailed regulatory mechanisms and functions of these two proteins remain unclear and warrant further *in vivo* and *in vitro* investigations.

STAR★METHODS

Detailed methods are provided in the online version of this paper and include the following:

- KEY RESOURCES TABLE
- RESOURCE AVAILABILITY
  - Lead contact
  - Materials availability
  - Data and code availability
- EXPERIMENTAL MODEL AND STUDY PARTICIPANT DETAILS
  - Ethical approval
  - Myocardial infarction mouse models
- METHOD DETAILS
  - Echocardiography
  - Histology and immunohistochemical staining
  - Cell cultures and knockdown or overexpression of *IFI-16* in AC16 myocytes
  - Cell hypoxia and nutrient deprivation
  - Western blot
  - Cellular immunofluorescence
  - Quantification of mitochondrial DNA (mtDNA) release
  - qPCR
  - Co-immunoprecipitation
- QUANTIFICATION AND STATISTICAL ANALYSIS

SUPPLEMENTAL INFORMATION

Supplemental information can be found online at https://doi.org/10.1016/j.isci.2024.110568.

ACKNOWLEDGMENTS

The authors would like to thank all the editors for their professional and meticulous reviews. This work was supported by the National Natural Science Foundation of China (8200150472), the Guangzhou Basic and Applied Basic Research Foundation (2023A04J0448), and a post-doctoral research project of Guangdong Provincial Hospital of Chinese Medicine (No. 10187).

AUTHOR CONTRIBUTIONS

B.C., Y.D., X.P., and Y.F. contributed to study conception and design. Y.D., L.C., and W.P. performed material preparation, data collection, and analysis. The first draft of the manuscript was written by B.C. and Y.D., and all authors commented on the previous versions of the manuscript. All the authors have read and approved the final version of the manuscript.

DECLARATION OF INTERESTS

The authors declare no competing interests.

Received: February 26, 2024
Revised: May 16, 2024
Accepted: July 19, 2024
Published: July 23, 2024

REFERENCES

1. White, H.D., Norris, R.M., Brown, M.A., Brandt, P.W., Whitlock, R.M., and Wild, C.J. (1987). Left ventricular end-systolic volume as the major determinant of survival after recovery from myocardial infarction. Circulation *76*, 44–51. https://doi.org/10.1161/01.cir.76.1.44.
2. Jung, M., Ma, Y., Iyer, R.P., DeLeon-Pennell, K.Y., Yabluchanskiy, A., Garrett, M.R., and Lindsey, M.L. (2017). IL-10 improves cardiac remodeling after myocardial infarction by stimulating M2 macrophage polarization and fibroblast activation. Basic Res. Cardiol. *112*, 33. https://doi.org/10.1007/s00395-017-0622-5.
3. Westman, P.C., Lipinski, M.J., Luger, D., Waksman, R., Bonow, R.O., Wu, E., and Epstein, S.E. (2016). Inflammation as a Driver of Adverse Left Ventricular Remodeling After Acute Myocardial Infarction. J. Am. Coll. Cardiol. *67*, 2050–2060. https://doi.org/10.1016/j.jacc.2016.01.073.
4. Thackeray, J.T., Hupe, H.C., Wang, Y., Bankstahl, J.P., Berding, G., Ross, T.L., Bauersachs, J., Wollert, K.C., and Bengel, F.M. (2018). Myocardial Inflammation Predicts Remodeling and Neuroinflammation After Myocardial Infarction. J. Am. Coll. Cardiol. *71*, 263–275. https://doi.org/10.1016/j.jacc.2017.11.024.
5. Fonseca, F.A., and Izar, M.C. (2022). Role of Inflammation in Cardiac Remodeling After Acute Myocardial Infarction. Front. Physiol. *13*, 927163. https://doi.org/10.3389/fphys.2022.927163.
6. Newby, L.K. (2019). Inflammation as a Treatment Target after Acute Myocardial Infarction. N. Engl. J. Med. *381*, 2562–2563. https://doi.org/10.1056/NEJMe1914378.
7. Bostan, M.M., Stătescu, C., Anghel, L., Serban, I.L., Cojocaru, E., and Sascau, R. (2020). Post-Myocardial Infarction Ventricular Remodeling Biomarkers-The Key Link between Pathophysiology and Clinic. Biomolecules *10*, 1587. https://doi.org/10.3390/biom10111587.
8. Hanna, A., and Frangogiannis, N.G. (2020). Inflammatory Cytokines and Chemokines as Therapeutic Targets in Heart Failure. Cardiovasc. Drugs Ther. *34*, 849–863. https://doi.org/10.1007/s10557-020-07071-0.
9. Ridker, P.M., Everett, B.M., Thuren, T., MacFadyen, J.G., Chang, W.H., Ballantyne, C., Fonseca, F., Nicolau, J., Koenig, W., Anker, S.D., et al. (2017). Antiinflammatory Therapy with Canakinumab for Atherosclerotic Disease. N. Engl. J. Med. Overseas. Ed. *377*, 1119–1131. https://doi.org/10.1056/NEJMoa1707914.
10. Bouabdallaoui, N., Tardif, J.C., Waters, D.D., Pinto, F.J., Maggioni, A.P., Diaz, R., Berry, C., Koenig, W., Lopez-Sendon, J., Gamra, H., et al. (2020). Time-to-treatment initiation of colchicine and cardiovascular outcomes after myocardial infarction in the Colchicine Cardiovascular Outcomes Trial (COLCOT). Eur. Heart J. *41*, 4092–4099. https://doi.org/10.1093/eurheartj/ehaa659.
11. Choubey, D., and Panchanathan, R. (2016). IFI16, an amplifier of DNA-damage response: Role in cellular senescence and aging-associated inflammatory diseases. Ageing Res. Rev. *28*, 27–36. https://doi.org/10.1016/j.arr.2016.04.002.
12. Choubey, D. (2022). Cytosolic DNA sensor IFI16 proteins: Potential molecular integrators of interactions among the aging hallmarks. Ageing Res. Rev. *82*, 101765. https://doi.org/10.1016/j.arr.2022.101765.
13. Fu, Q., He, Q., Dong, Q., Xie, J., Geng, Y., Han, H., Huang, Y., Lu, J., Zeng, Z., Wang, W., et al. (2022). The role of cyclic GMP-AMP synthase and Interferon-I-inducible protein 16 as candidatebiomarkers of systemic lupus erythematosus. Clin. Chim. Acta *524*, 69–77. https://doi.org/10.1016/j.cca.2021.11.003.
14. Vanhove, W., Peeters, P.M., Staelens, D., Schraenen, A., Van der Goten, J., Cleynen, I., De Schepper, S., Van Lommel, L., Reynaert, N.L., Schuit, F., et al. (2015). Strong Upregulation of AIM2 and IFI16 Inflammasomes in the Mucosa of Patients with Active Inflammatory Bowel Disease. Inflamm. Bowel Dis. *21*, 2673–2682. https://doi.org/10.1097/mib.0000000000000535.
15. Nissen, S.K., Højen, J.F., Andersen, K.L.D., Kofod-Olsen, E., Berg, R.K., Paludan, S.R., Østergaard, L., Jakobsen, M.R., Tolstrup, M., and Mogensen, T.H. (2014). Innate DNA sensing is impaired in HIV patients and IFI16 expression correlates with chronic immune activation. Clin. Exp. Immunol. *177*, 295–309. https://doi.org/10.1111/cei.12317.
16. Dunphy, G., Flannery, S.M., Almine, J.F., Connolly, D.J., Paulus, C., Jønsson, K.L., Jakobsen, M.R., Nevels, M.M., Bowie, A.G., and Unterholzner, L. (2018). Non-canonical Activation of the DNA Sensing Adaptor STING by ATM and IFI16 Mediates NF-κB Signaling after Nuclear DNA Damage. Mol. Cell *71*, 745–760.e5. https://doi.org/10.1016/j.molcel.2018.07.034.
17. Chunfa, L., Xin, S., Qiang, L., Sreevatsan, S., Yang, L., Zhao, D., and Zhou, X. (2017). The Central Role of IFI204 in IFN-beta Release and Autophagy Activation during *Mycobacterium bovis* Infection. Front. Cell. Infect. Microbiol. *7*, 169. https://doi.org/10.3389/fcimb.2017.00169.
18. Cai, H., Yan, L., Liu, N., Xu, M., and Cai, H. (2020). IFI16 promotes cervical cancer progression by upregulating PD-L1 in immunomicroenvironment through STING-TBK1-NF-kB pathway. Biomed. Pharmacother. *123*, 109790. https://doi.org/10.1016/j.biopha.2019.109790.
19. Jaén, R.I., Val-Blasco, A., Prieto, P., Gil-Fernández, M., Smani, T., López-Sendón, J.L., Delgado, C., Boscá, L., and Fernández-Velasco, M. (2020). Innate Immune Receptors, Key Actors in Cardiovascular Diseases. JACC. Basic Transl. Sci. *5*, 735–749. https://doi.org/10.1016/j.jacbts.2020.03.015.
20. Kim, J., Gupta, R., Blanco, L.P., Yang, S., Shteinfer-Kuzmine, A., Wang, K., Zhu, J., Yoon, H.E., Wang, X., Kerkhofs, M., et al. (2019). VDAC oligomers form mitochondrial pores to release mtDNA fragments and promote lupus-like disease. Science *366*, 1531–1536. https://doi.org/10.1126/science.aav4011.
21. Li, D., Xie, L., Qiao, Z., Mai, S., Zhu, J., Zhang, F., Chen, S., Li, L., Shen, F., Qin, Y., et al. (2021). STING-mediated degradation of IFI16 negatively regulates apoptosis by inhibiting p53 phosphorylation at serine 392. J. Biol. Chem. *297*, 100930. https://doi.org/10.1016/j.jbc.2021.100930.
22. Higashikuni, Y., Liu, W., Numata, G., Tanaka, K., Fukuda, D., Tanaka, Y., Hirata, Y., Imamura, T., Takimoto, E., Komuro, I., and Sata, M. (2023). NLRP3 Inflammasome Activation Through Heart-Brain Interaction Initiates Cardiac Inflammation and Hypertrophy During Pressure Overload. Circulation *147*, 338–355. https://doi.org/10.1161/CIRCULATIONAHA.122.060860.
23. Onódi, Z., Ruppert, M., Kucsera, D., Sayour, A.A., Toth, V.E., Koncsos, G., Novak, J., Brenner, G.B., Makkos, A., Baranyai, T., et al. (2021). AIM2-driven inflammasome activation in heart failure. Cardiovasc. Res. *117*, 2639–2651. https://doi.org/10.1093/cvr/cvab202.
24. Qian, J., Liang, S., Wang, Q., Xu, J., Huang, W., Wu, G., and Liang, G. (2023). Toll-like receptor-2 in cardiomyocytes and macrophages mediates isoproterenol-induced cardiac inflammation and remodeling. FASEB J. *37*, e22740. https://doi.org/10.1096/fj.202201345R.
25. Yoshida, K., Abe, K., Ishikawa, M., Saku, K., Shinoda-Sakamoto, M., Ishikawa, T., Watanabe, T., Oka, M., Sunagawa, K., and Tsutsui, H. (2019). Inhibition of TLR9-NF-kappaB-mediated sterile inflammation improves pressure overload-induced right ventricular dysfunction in rats. Cardiovasc. Res. *115*, 658–668. https://doi.org/10.1093/cvr/cvy209.
26. Ueda, H., Yamaguchi, O., Taneike, M., Akazawa, Y., Wada-Kobayashi, H., Sugihara, R., Yorifuji, H., Nakayama, H., Omiya, S., Murakawa, T., et al. (2019). Administration of a TLR9 Inhibitor Attenuates the Development and Progression of Heart Failure in Mice. JACC. Basic Transl. Sci. *4*, 348–363. https://doi.org/10.1016/j.jacbts.2019.01.002.
27. Hu, D., Cui, Y.X., Wu, M.Y., Li, L., Su, L.N., Lian, Z., and Chen, H. (2020). Cytosolic DNA sensor cGAS plays an essential pathogenetic role in pressure overload-induced heart failure. Am. J. Physiol. Heart Circ. Physiol. *318*. H1525-h1537. https://doi.org/10.1152/ajpheart.00097.2020.
28. Jiang, Z., Wei, F., Zhang, Y., Wang, T., Gao, W., Yu, S., Sun, H., Pu, J., Sun, Y., Wang, M., et al. (2021). IFI16 directly senses viral RNA and enhances RIG-I transcription and activation to restrict influenza virus infection. Nat. Microbiol. *6*, 932–945. https://doi.org/10.1038/s41564-021-00907-x.
29. Xue, M., Li, D., Wang, Z., Mi, L., Cao, S., Zhang, L., and Kong, X. (2021). IFI16 contributes to the pathogenesis of abdominal aortic aneurysm by regulating the caspase-1/IL-1beta/MCPIP1 pathway. Life Sci. *265*, 118752. https://doi.org/10.1016/j.lfs.2020.118752.
30. Hansen, K., Prabakaran, T., Laustsen, A., Jørgensen, S.E., Rahbæk, S.H., Jensen, S.B., Nielsen, R., Leber, J.H., Decker, T., Horan, K.A., et al. (2014). Listeria monocytogenes induces IFNβ expression through an IFI16-cGAS- and STING-dependent pathway. EMBO J. *33*, 1654–1666. https://doi.org/10.15252/embj.201488029.
31. Chiliveru, S., Rahbek, S.H., Jensen, S.K., Jørgensen, S.E., Nissen, S.K., Christiansen, S.H., Mogensen, T.H., Jakobsen, M.R., Iversen, L., Johansen, C., and Paludan, S.R. (2014). Inflammatory cytokines break down intrinsic immunological tolerance of human primary keratinocytes to cytosolic DNA. J. Immunol. *192*, 2395–2404. https://doi.org/10.4049/jimmunol.1302120.
32. Li, X.Q., Yu, Q., Fang, B., Zhang, Z.L., and Ma, H. (2019). Knockdown of the AIM2 molecule attenuates ischemia-reperfusion-induced spinal neuronal pyroptosis by inhibiting AIM2 inflammasome activation and subsequent release of cleaved caspase-1 and IL-1beta.

Neuropharm. *160*, 107661. https://doi.org/10.1016/j.neuropharm.2019.05.038.
33. Liu, Y., Yan, W., Tohme, S., Chen, M., Fu, Y., Tian, D., Lotze, M., Tang, D., and Tsung, A. (2015). Hypoxia induced HMGB1 and mitochondrial DNA interactions mediate tumor growth in hepatocellular carcinoma through Toll-like receptor 9. J. Hepatol. *63*, 114–121. https://doi.org/10.1016/j.jhep.2015.02.009.
34. Paludan, S.R., Reinert, L.S., and Hornung, V. (2019). DNA-stimulated cell death: implications for host defence, inflammatory diseases and cancer. Nat. Rev. Immunol. *19*, 141–153. https://doi.org/10.1038/s41577-018-0117-0.
35. Xian, H., Watari, K., Sanchez-Lopez, E., Offenberger, J., Onyuru, J., Sampath, H., Ying, W., Hoffman, H.M., Shadel, G.S., and Karin, M. (2022). Oxidized DNA fragments exit mitochondria via mPTP- and VDAC-dependent channels to activate NLRP3 inflammasome and interferon signaling. Immunity *55*, 1370–1385.e8. https://doi.org/10.1016/j.immuni.2022.06.007.
36. McArthur, K., Whitehead, L.W., Heddleston, J.M., Li, L., Padman, B.S., Oorschot, V., Geoghegan, N.D., Chappaz, S., Davidson, S., San Chin, H., et al. (2018). BAK/BAX macropores facilitate mitochondrial herniation and mtDNA efflux during apoptosis. Science *359*, eaao6047. https://doi.org/10.1126/science.aao6047.
37. Takahashi, M. (2019). Role of NLRP3 Inflammasome in Cardiac Inflammation and Remodeling after Myocardial Infarction. Biol. Pharm. Bull. *42*, 518–523. https://doi.org/10.1248/bpb.b18-00369.
38. Monroe, K.M., Yang, Z., Johnson, J.R., Geng, X., Doitsh, G., Krogan, N.J., and Greene, W.C. (2014). IFI16 DNA sensor is required for death of lymphoid CD4 T cells abortively infected with HIV. Science *343*, 428–432. https://doi.org/10.1126/science.1243640.
39. Unterholzner, L., Keating, S.E., Baran, M., Horan, K.A., Jensen, S.B., Sharma, S., Sirois, C.M., Jin, T., Latz, E., Xiao, T.S., et al. (2010). IFI16 is an innate immune sensor for intracellular DNA. Nat. Immunol. *11*, 997–1004. https://doi.org/10.1038/ni.1932.
40. Xiong, R., Li, N., Chen, L., Wang, W., Wang, B., Jiang, W., and Geng, Q. (2021). STING protects against cardiac dysfunction and remodelling by blocking autophagy. Cell Commun. Signal. *19*, 109. https://doi.org/10.1186/s12964-021-00793-0.
41. Dong, R., Zhang, M., Hu, Q., Zheng, S., Soh, A., Zheng, Y., and Yuan, H. (2018). Galectin-3 as a novel biomarker for disease diagnosis and a target for therapy (Review). Int. J. Mol. Med. *41*, 599–614. https://doi.org/10.3892/ijmm.2017.3311.
42. Blanda, V., Bracale, U.M., Di Taranto, M.D., and Fortunato, G. (2020). Galectin-3 in Cardiovascular Diseases. Int. J. Mol. Sci. *21*, 9232. https://doi.org/10.3390/ijms21239232.
43. Chow, S.L., Maisel, A.S., Anand, I., Bozkurt, B., de Boer, R.A., Felker, G.M., Fonarow, G.C., Greenberg, B., Januzzi, J.L., Jr., Kiernan, M.S., et al. (2017). Role of Biomarkers for the Prevention, Assessment, and Management of Heart Failure: A Scientific Statement From the American Heart Association. Circulation *135*, e1054–e1091. https://doi.org/10.1161/cir.0000000000000490.
44. de Boer, R.A., van der Velde, A.R., Mueller, C., van Veldhuisen, D.J., Anker, S.D., Peacock, W.F., Adams, K.F., and Maisel, A. (2014). Galectin-3: a modifiable risk factor in heart failure. Cardiovasc. Drugs Ther. *28*, 237–246. https://doi.org/10.1007/s10557-014-6520-2.
45. Ho, J.E., Liu, C., Lyass, A., Courchesne, P., Pencina, M.J., Vasan, R.S., Larson, M.G., and Levy, D. (2012). Galectin-3, a marker of cardiac fibrosis, predicts incident heart failure in the community. J. Am. Coll. Cardiol. *60*, 1249–1256. https://doi.org/10.1016/j.jacc.2012.04.053.
46. Sharma, U.C., Pokharel, S., van Brakel, T.J., van Berlo, J.H., Cleutjens, J.P.M., Schroen, B., André, S., Crijns, H.J.G.M., Gabius, H.J., Maessen, J., and Pinto, Y.M. (2004). Galectin-3 marks activated macrophages in failure-prone hypertrophied hearts and contributes to cardiac dysfunction. Circulation *110*, 3121–3128. https://doi.org/10.1161/01.cir.0000147181.65298.4d.
47. Yu, L., Ruifrok, W.P.T., Meissner, M., Bos, E.M., van Goor, H., Sanjabi, B., van der Harst, P., Pitt, B., Goldstein, I.J., Koerts, J.A., et al. (2013). Genetic and pharmacological inhibition of galectin-3 prevents cardiac remodeling by interfering with myocardial fibrogenesis. Circ. Heart Fail. *6*, 107–117. https://doi.org/10.1161/circheartfailure.112.971168.
48. Xin, H., Curry, J., Johnstone, R.W., Nickoloff, B.J., and Choubey, D. (2003). Role of IFI 16, a member of the interferon-inducible p200-protein family, in prostate epithelial cellular senescence. Oncogene *22*, 4831–4840. https://doi.org/10.1038/sj.onc.1206754.
49. Rathod, K.S., Kapil, V., Velmurugan, S., Khambata, R.S., Siddique, U., Khan, S., Van Eijl, S., Gee, L.C., Bansal, J., Pitrola, K., et al. (2017). Accelerated resolution of inflammation underlies sex differences in inflammatory responses in humans. J. Clin. Invest. *127*, 169–182. https://doi.org/10.1172/jci89429.
50. Enzan, N., Matsushima, S., Ikeda, S., Okabe, K., Ishikita, A., Yamamoto, T., Sada, M., Miyake, R., Tsutsui, Y., Nishimura, R., et al. (2023). ZBP1 Protects Against mtDNA-Induced Myocardial Inflammation in Failing Hearts. Circ. Res. *132*, 1110–1126. https://doi.org/10.1161/circresaha.122.322227.
51. Ling, Y., Chen, G., Deng, Y., Tang, H., Ling, L., Zhou, X., Song, X., Yang, P., Liu, Y., Li, Z., et al. (2016). Polydatin post-treatment alleviates myocardial ischaemia/reperfusion injury by promoting autophagic flux. Clin. Sci. *130*, 1641–1653. https://doi.org/10.1042/cs20160082.
52. Li, L., Gao, P., Tang, X., Liu, Z., Cao, M., Luo, R., Li, X., Wang, J., Lin, X., Peng, C., et al. (2022). CB1R-stabilized NLRP3 inflammasome drives antipsychotics cardiotoxicity. Signal Transduct. Target. Ther. *7*, 190. https://doi.org/10.1038/s41392-022-01018-7.

STAR★METHODS

KEY RESOURCES TABLE

REAGENT or RESOURCE	SOURCE	IDENTIFIER
Antibodies		
IFI-16	Affinity	Cat#DF6750; RRID: AB_2838712
IFI-16	Cell Signaling Technology	Cat#14970; RRID: AB_2798669
IFI-204	ABCAM	Cat#ab307201; RRID: AB_3166180
ASC	Santa Cruz	Cat#sc-514414; RRID: AB_2737351
Caspase-1/Cleaved-caspase-1	Affinity	Cat#AF4022; RRID: AB_2845464
Caspase-1	ABCAM	Cat#ab207802; RRID: AB_2889889
GSDMD/cleaved-GSDMD	Affinity	Cat#AF4012; RRID: AB_2846776
α-SMA	Proteintech	Cat#67735-1; RRID: AB_2918504
TNF-α	Proteintech	Cat#60291-1; RRID: AB_2833255
Galectin-3	Proteintech	Cat#60207-1; RRID: AB_10951109
GAPDH	BOSTER	Cat#BM3896; RRID: AB_3166181
P53	Proteintech	Cat#60283-2; RRID: AB_2881401
Cleaved-caspase-9	Cell Signaling Technology	Cat# 9507; RRID: AB_2228625
β-actin	Proteintech	Cat#66009-1; RRID: AB_2687938
TNNT2	Proteintech	Cat# 15513-1-AP; RRID: AB_2206563
Critical commercial assay		
Mito-Tracker Red CMXRos	Beyotime	Cat#C1053
DAPI	Beyotime	Cat#C1005
CO-IP test Kit	Thermo Fisher	Cat#26149
SYBR Green Pro Taq HS	Accurate biology	Cat#AG11701
Silver staining test kit	Beyotime	Cat#P0017
Proteinase K	Accurate biology	Cat#AG12306
VBIT-4	MREDA	Cat#M204494
Digitonin	MREDA	Cat#M98985
Oligonucleotides		
See Table S4 for a list of oligonucleotides		
Software and algorithms		
ImageJ	ImageJ	https://imagej.nih.gov/ij/
Adobe Illustrator	Adobe	https://www.adobe.com/es/
Adobe Photoshop	Adobe	https://www.adobe.com/es/
Prism	GraphPad	https://www.graphpad.com/

RESOURCE AVAILABILITY

Lead contact

Further information and requests for resources and reagents should be directed to and will be fulfilled by the lead contact, Bojun Chen (gzcbj@gzucm.edu.cn).

Materials availability

This study did not generate new unique reagents.

Data and code availability

- Data: All data reported will be shared by the lead contact upon request.
- Code: This paper does not report original code.
- Additional information required to analyze the data reported in this paper is available from the lead contact upon request.

EXPERIMENTAL MODEL AND STUDY PARTICIPANT DETAILS

Ethical approval

The experimental procedures adhered to the guidelines outlined in the National Institutes of Health Guide for the Care and Use of Laboratory Animals. Ethical approval for this study was obtained from the Research Institute of Animal Protection and Use Committee of the Guangdong Provincial Hospital of Chinese Medicine (SCXK [Yue] 2021045).

Myocardial infarction mouse models

A recent study considered sex differences in inflammatory responses[49] by exclusively using male mice and excluding female mice to mitigate potential sex-related effects on outcomes.[50] Male C57BL/6 mice, aged 6–8 weeks, were obtained from the Animal Research Laboratory of Guangdong Province, Guangzhou, China. All animals were randomly allocated to different experimental groups. A previously established method involving ligation of the left coronary artery was employed to induce MI.[51] The mice were anesthetized with 1–2% isoflurane. Oral intubation and mechanical ventilation were maintained throughout the procedure. A left thoracotomy was performed, followed by opening of the pericardium. Subsequently, the ligature was securely placed around the left anterior descending coronary artery. For the sham operations, the ligature was not tightened. Following the surgical intervention, the mice were returned to their respective cages.

To achieve knockdown of *Ifi-204* expression in mice, adeno-associated virus (AAV) vectors were utilized. Specifically, the AAV vectors named pAAV-U6-shRNA (NC2)-CMV-EGFP-WPRE (referred to as AAV-Ctrl) or pAAV-U6-shRNA (ifi204)-CMV-EGFP-WPRE (referred to as AAV-IFI204) were injected into the LV[52] at a viral copy number of 2×10^{11} using a 100-μL microinjector equipped with a 34G 1.2 mm four-needle head (COMPUVON, Hengshui, China). Hearts were harvested from the mice after cervical dissection and euthanasia. Horizontal cuts were made near the ligatures, and immunohistochemistry experiments were performed after fixation of the apex. 1-2 mm whole-circle heart tissue samples near the ligature line were obtained for protein extraction, intended for western blot analysis.

METHOD DETAILS

Echocardiography

Echocardiography was conducted on the anesthetized mice utilizing the Vevo 2100 system (VisualSonics, Toronto, Canada), equipped with a transducer operating at 40 MHz. Anesthesia was administered using pentobarbital (50 mg/kg). The imaging procedure involved acquiring two-dimensional parasternal short-axis views of the heart using an M-mode echocardiogram recorded at the level of the papillary muscles. The acquired images were subsequently analyzed using Vevo 2100 software (version 1.1.1, VisualSonics, Toronto, Canada). Part of the original images are in Figure S10.

Histology and immunohistochemical staining

Immunohistochemical staining was employed to examine the percentage of fibrosis and inflammation in the heart sections of mice using hematoxylin-eosin and Masson staining. The stained sections were observed and analyzed under a microscope (Olympus, Tokyo, Japan) to visualize and examine the staining patterns. After three thorough washes with phosphate-buffered saline (PBS), tissue sections were stained with WGA, following the manufacturer's guidelines. Subsequently, the sections were incubated with anti-IFI-16 (Affinity Biosciences, 1:400) and anti-cleaved caspase-1 (Affinity Biosciences, 1:400) primary antibodies overnight at 4°C. Following primary antibody incubation, the sections were allowed to equilibrate at 37°C for 30 min. Subsequently, fluorescence-labeled sections underwent an additional incubation step with an appropriate secondary antibody, namely, a 1:200 dilution of goat anti-rabbit Cy3-tagged antibody, for 45 min at 37°C. The sections were washed and mounted using 4′,6-diamidino-2-phenylindole (DAPI) and stored in a light-protected environment at 4°C until imaging. Fluorescence was observed under a fluorescence microscope (Olympus, Tokyo, Japan) or laser scanning confocal microscope (ZEISS LSM 710). Images of the designated tissue sections were analyzed using ImageJ 1.53 to quantify immunofluorescence.

Cell cultures and knockdown or overexpression of *IFI-16* in AC16 myocytes

The AC16 human cardiac cell line was cultured in Dulbecco's Modified Eagle's Medium and Ham's F12 Nutrient Mixture (DMEM/F12; Thermo, Massachusetts, US), supplemented with 10% fetal bovine serum (FBS; Gibco, USA), and antibiotics (100 U/mL penicillin and 100 μg/mL streptomycin; Thermo, Massachusetts, US). To achieve knockdown or overexpression of *IFI16* in AC16 myocytes, lentiviruses were prepared using the following plasmids: IFI16-shRNA-pLVX-PURO for knockdown and IFI16-pCDH-GFP+PURO for overexpression. The detailed information of oligonucleotides was provided in Table S4. These plasmids were co-transfected with helper plasmids psPAX2 and pMD 2. G into 293T cells and incubated for 48 h. Subsequently, the virus-containing supernatant was collected and used to infect AC16 myocytes. Following infection, cells were subjected to puromycin selection to establish stable cell lines for further experimentation and analysis.

Cell hypoxia and nutrient deprivation

The AC16 myocytes were maintained in a controlled incubation environment at a temperature of 37°C with 5% CO_2 and humidity. The following steps were performed to induce hypoxia. The cells were rinsed thrice with D-Hank's solution. Subsequently, 4 mL of D-hank solution was added to each flask containing the cells and placed in a Tri-gas incubator that had been equilibrated with a gas mixture of 1% O_2, 5% CO_2, and 94% N_2. The cells were incubated in this humidified environment at 37°C within the tri-gas incubator for a 2–6 h. This reduced oxygen environment mimicked hypoxia, allowing the investigation of cellular responses under hypoxic conditions in AC16 myocytes.

Western blot

Samples were collected from post-MI mouse hearts and AC16 cells subjected to hypoxia and nutrient deprivation. Using a BCA assay, the protein concentration in each sample was determined. A total of 20 μg protein from each sample was mixed with a loading buffer (Beyotime, China) and subjected to sodium dodecyl sulfate-polyacrylamide gel electrophoresis (SDS-PAGE) for separation. The separated proteins were transferred onto PVDF membranes (Millipore, Billerica, MA, USA). After blocking with skim milk, the membranes were washed and incubated overnight at 4°C with the following primary antibodies: rabbit anti-IFI-16 (Affinity Biosciences, 1:1000), anti-caspase-1 (Abcam, 1:1000), anti-cleaved-caspase-1 (Affinity Biosciences, 1:1000), anti-Gasdermin D (GSDMD, Affinity Biosciences, 1:1000), anti-cleaved- GSDMD (Abcam, 1:1000), anti-α-smooth muscle actin (α-SMA, Bioss, 1:1000), anti-GAPDH (Boster, 1:4000), mouse anti-apoptosis-associated speck-like protein containing CARD (ASC, Santa Cruz, 1:100), anti-tumor necrosis factor-α (TNF-α, Proteintech, 1:1000), anti-Galectin3 (Proteintech, 1:1000), Cleaved-caspase9 (CST, 1:1000) and anti-p53 (Proteintech, 1:1000). After three washes, the membranes were incubated with a secondary antibody (Boster, China, 1:5000) and chemiluminescence was assessed using a detection system (Millipore). The optical density of the protein bands were measured using ImageJ 1.53 software. Relative protein expression levels were calculated by normalizing to GAPDH. Each experiment was repeated thrice to ensure reproducibility.

Cellular immunofluorescence

Following hypoxia, myocytes were fixed with 4% paraformaldehyde for 20 min at room temperature. Subsequently, the cells were washed thrice with PBS and permeabilized with 0.25% Triton X-100 for 5 min. The cells were washed again with PBS. To block nonspecific binding, the cells were incubated with 3% FBS (BSA) at room temperature for 1 h. Following this, the cells were incubated overnight at 4°C with primary antibodies. After incubation, the cells were washed thrice with PBS. Subsequently, the cells were incubated with fluorescein isothiocyanate-tagged (FITC) secondary antibodies (Boster, China, 1:200) for 2 h at room temperature. Finally, the myocytes were visualized using a laser scanning confocal microscope (ZEISS LSM 710). Immunofluorescence was quantified using ImageJ 1.53.

Quantification of mitochondrial DNA (mtDNA) release

To quantify the release of mtDNA, the following method was used as previously reported.[20] A total of 2×10^6 myocytes were resuspended in 170 μL of digitonin buffer, composed of 150 mM NaCl, 50 mM HEPES (pH 7.4), and 25 μg/mL digitonin (MREDA, Beijing, China). The cell homogenates were then incubated on a rotator for 10 min at room temperature, followed by centrifugation at 16,000×g for 25 min at 4°C. The supernatant (cmtDNA) was diluted 1:20, and a 1:20 dilution of this supernatant was utilized for quantitative PCR (qPCR) analysis. Furthermore, the pellet obtained from the centrifugation step was resuspended in 340 μL of lysis buffer containing proteinase K (AG12306, Accurate Biology, Hunan, China). The sample was then heated at 95°C for 5 min to inactivate the proteinase K, and the resulting sample was used for qPCR analysis with mtDNA-specific primers, detailed information is provided in Table S4.

qPCR

SYBR Green Master Mix (Rox Plus) (AG11718; Accurate Biology, Hunan, China) was used for PCR amplification. The cmtDNA present in the supernatant was normalized to the total mtDNA obtained from the pellet for each sample. Real-time PCR results were calculated using the 2^(-ΔΔCt) method. In this study, the primer pairs used were synthesized by Shanghai General Biotech Co., Ltd. The specific primer information is provided in STAR Methods.

Co-immunoprecipitation

Co-IP experiments were conducted using AC16 myocytes as a cellular model. The Co-IP procedure followed the manufacturer's guidelines and was performed using the Pierce Immunoprecipitation Kit (26149, Thermo Fisher Scientific). Subsequently, the eluted samples were subjected to SDS-PAGE and visualized using silver staining (P0017s, Beyotime, China). Following this initial analysis, protein samples that satisfied the predefined quality standards were retained for further experimentation.

QUANTIFICATION AND STATISTICAL ANALYSIS

Data are presented as the mean ± SEM (standard error of the mean). Statistical comparisons between the two groups were conducted using the unpaired Student's t test. Experiments with more than two groups were evaluated using a one-way analysis of variance followed by Fisher's LSD test. Statistical significance was set at 0.05 ($p < 0.05$). Statistical analyses were performed using GraphPad Prism 10.0 software (GraphPad Software Inc.).